Photoluminescence studies on structural defects and room temperature ferromagnetism in Ni and Ni–H doped ZnO nanoparticles

Liu-Niu Tong, Teng Cheng, Huai-Bin Han, Jin-Lian Hu, Xian-Mei He, Yan Tong, and Claus M. Schneider

Citation: Journal of Applied Physics **108**, 023906 (2010);
View online: https://doi.org/10.1063/1.3460644
View Table of Contents: http://aip.scitation.org/toc/jap/108/2
Published by the American Institute of Physics

Photoluminescence studies on structural defects and room temperature ferromagnetism in Ni and Ni–H doped ZnO nanoparticles

Liu-Niu Tong,[1,a)] Teng Cheng,[1] Huai-Bin Han,[1] Jin-Lian Hu,[1] Xian-Mei He,[2] Yan Tong,[3] and Claus M. Schneider[4]

[1]*Anhui Key Laboratory of Metal Materials and Processing, School of Material Science and Engineering, Anhui University of Technology, Ma-An-Shan, 243002 Anhui, China*
[2]*School of Mathematics and Physics, Anhui University of Technology, Ma-An-Shan, 243002 Anhui, China*
[3]*School of Mechanical Engineering, Anhui University of Technology, Ma-An-Shan, 243002 Anhui, China*
[4]*Institute of Solid State Research IFF-9, Research Centre Jülich, D-52425 Jülich, Germany*

(Received 16 February 2010; accepted 8 June 2010; published online 20 July 2010)

We explore the effects of hydrogenated annealing on the crystal structure, room temperature ferromagnetism (RT-FM) and photoluminescence (PL) properties of Ni-doped ZnO ($Zn_{1-x}Ni_xO$, $x=0.0$ to 0.2) nanoparticles prepared by a sol-gel method. The x-ray photoelectron spectra and x-ray diffraction data provide evidence that Ni has been incorporated into the wurtzite ZnO lattice as Ni^{2+} ions substituting for Zn^{2+} ions at $x \leq 0.05$. A secondary phase of NiO type begins to form inside ZnO when $x > 0.05$ and segregates from ZnO host lattice at $x=0.2$, leading to a large variation in the lattice constants of ZnO. The magnetization measurements show that the saturation magnetization (M_s) increases with increasing Ni concentration in the single-phase $Zn_{1-x}Ni_xO$ ($x \leq 0.05$) nanoparticles. The secondary phase formation reduces the magnetization of $Zn_{1-x}Ni_xO$ ($x=0.1$ and 0.15), while the segregation of NiO from the ZnO lattice at $x=0.2$ is accompanied by a large increase in M_s again. The PL measurements show that the UV emission intensity of single-phase $Zn_{1-x}Ni_xO$ ($x \leq 0.05$) nanoparticles increases with a blueshift in the UV emission line when the Ni concentration increases, while the dominant green emission intensity decreases with increasing Ni dopant. The PL data strongly suggest that the FM in single-phase $Zn_{1-x}Ni_xO$ ($x \leq 0.05$) nanoparticles is intrinsically correlated with a doping induced increase in the electron concentration in the conduction band of Ni-doped ZnO. After H_2-annealing, the single-phase $Zn_{1-x}Ni_xO:H$ ($x \leq 0.05$) nanoparticles show increases in both coercivity and saturation magnetization. The PL and diffuse reflectance spectra suggest that hydrogen-related shallow donors and an improved sample quality may be responsible for the H_2-annealing induced enhancement of the RT-FM. The obvious correlation between FM and carrier concentration in Ni and Ni–H doped ZnO points towards a mechanism of carrier-mediated FM for Ni-doped ZnO diluted magnetic semiconductors. © *2010 American Institute of Physics*. [doi:10.1063/1.3460644]

I. INTRODUCTION

Diluted magnetic semiconductors (DMSs) have recently attracted considerable research interest, not only because of their potential applications as spin-based materials in spintronics, but also because of their fundamental role in understanding complex exchange mechanisms in magnetism.[1,2] Since Dietl *et al.*[3] predicted within a mean-field approach that stable ferromagnetic configurations arising from carrier-mediated exchange interactions might exist in p-type Mn-doped ZnO, many efforts have been devoted to the search for high Curie temperature ferromagnetism (FM) in transition metal (TM)-doped wide-band semiconducting oxides such as TiO_2, ZnO, and SnO_2.[4–6] Recently, some experimental evidence for a high-temperature ferromagnetic state in the Ni-doped ZnO system has been reported, in consistency with theoretical predictions.[7,8] The experimental observations are based on Ni-doped ZnO films[9,10] and aggregated nanocrystals of Ni^{2+}:ZnO.[11,12] However, there are still many inconsistencies and controversies with respect to the origin of the magnetic properties described for Ni-doped ZnO in the literature. For instance, some authors[10,13] observed in their Ni-doped ZnO films that the saturation magnetic moments decrease with the Ni-doping concentration. Meanwhile, Thota *et al.*[14] found that the magnetization value of $Zn_{1-x}Ni_xO/ZnO$ ($0.01 \leq x \leq 0.163$) bilayers increases with an increase in the nickel content. Hou *et al.*[15] reported the saturation magnetization to first increase and then decrease as the Ni concentration increases. When the Ni concentration approaches 0.04, the saturation magnetization reaches a maximum value of 0.43 μ_B/Ni. El-Hilo *et al.*[16] reported that Ni-doped powders containing a low Ni content ($x=1, 4.3, 7.4$ at. % Ni) exhibit superparamagnetic behaviour while a sample with 22.5 at. % Ni shows clear FM at room temperature (RT). In contrast to the above cases, there are also reports of the absence of RT-FM in ZnO:Ni films.[17,18] Up to now, it is not clear whether the observed RT-FM in Ni-doped ZnO is a truly intrinsic property or is related to the formation of secondary phases such as magnetic clusters.[19–22]

a)Electronic mail: lntong@ahut.edu.cn.

Generally, experiments show that the magnetic properties of ZnO:Ni are sensitive to the crystal structure and concentration of native or artificially introduced defects, which in turn depend strongly on the preparation method and procedure. It has been suggested that the codoping with hydrogen as mediating agent could be an effective way to tune the concentration of mobile carriers or defects and to enhance the FM in ZnO-based DMSs.[7,23] Experimental evidence of hydrogen induced enhancement of the FM was indeed observed previously in some TM-doped ZnO systems for TM =Co,[24–27] Cr,[28] and V.[29] However, the effect of codoping with hydrogen on the FM in the Ni-doped ZnO system remains unclear. In the literature, several mechanisms have been proposed to address the effect of H-impurities on the magnetic properties in TM-doped ZnO. It was shown by Deka and Joy[25] for ZnO:Co that the process of hydrogen reduction during H_2-annealing does not affect the substituted Co^{2+} ions inside the wurtzite crystal lattice but can reduce Co_3O_4 to metal Co clusters which then contribute to the FM. While Hsu *et al.*[26] demonstrated that the hydrogen diffuses into the grain interior and causes more defects in ZnO:Co which result in a larger saturation magnetization. Recently, a multicenter bond shallow donor defect with hydrogen occupying in an oxygen vacancy (H_O) was proposed to be responsible for the hydrogen-induced magnetization increase.[28] Apparently, the role of H-impurities on the FM in ZnO-based DMSs is still far from being understood. In order to understand the changes in the magnetic properties of TM-doped ZnO induced by hydrogen, more information on the microscopic mechanisms is needed.

In this paper, we present a systematic study on the effects of Ni and Ni–H doping on the crystal structure and RT-FM of ZnO nanoparticles prepared by a sol-gel method. The systems were characterized by combining x-ray photoelectron spectroscopy (XPS), x-ray diffraction (XRD), photoluminescence (PL) spectra, diffuse reflectance (DR) spectra, and magnetization measurements. We find a clear correlation between the structural parameters, FM, and optical properties in Ni and Ni–H doped ZnO nanoparticles, which provides strong evidence that there may be a mechanism of carrier-mediated FM for Ni-doped ZnO DMSs.

II. EXPERIMENTAL DETAILS

Ni-doped ZnO samples were synthesized by the sol-gel technique. Zinc acetate $[Zn(Ac)_2 \cdot 2H_2O]$, nickel nitrate $[Ni(NO_3)_2 \cdot 6H_2O]$, and ethylene glycol were employed as raw starting materials. All chemicals used were of analytical grade purity. The chemical ingredients were weighted in stoichiometric proportions, dissolved in about 100 ml of ethylene glycol, and stirred continuously on a magnetic stirrer. A few drops (about 8 ml) of ethanolamine were added in order to make the resulting solution completely transparent. The temperature of the solution was raised in small steps (5 °C after every 2 h). After a gel has been formed, the temperature was further raised to 100 °C to boil off any water. After heat treatment at 250 °C the resultant substances were subsequently ground into fine powders, which served as precursors for the next step. The ZnNiO samples were produced through calcining the precursors at 875 K for 6 h in air and then cooling them down in the furnace. The ZnNiO:H samples were obtained by annealing the as-synthesized powders in H_2 at 400 °C and 1 atm for about 2 h. The crystal structure of the samples was characterized by means of XRD, using an x-ray diffractometer with Cu $K\alpha$ radiation. The valence states of Ni in the ZnO matrix were analyzed using XPS, using Mg $K\alpha$ line (1253.6 eV) excitation (Perkin Elmer PHI 1600 ESCA system). Magnetization measurements as a function of the magnetic field were carried out using a vibration sample magnetometer (VSM). The PL spectra were acquired using a cw He–Cd laser as excitation source (λ=325 nm, power ~3 mW). The DR spectra at normal incidence taken from the powder samples were measured by means of a ultraviolet visible (UV-Vis) spectrophotometer (SHIMADZU UV2550). All the measurements were carried out at RT.

III. RESULTS AND ANALYSIS

A. Structural characteristics by x-rays

Figure 1(a) shows the XRD patterns of as-synthesized $Zn_{1-x}Ni_xO$ (x=0 to 0.2) nanoparticles. The patterns reveal that all the samples studied are polycrystalline with a hexagonal wurtzite ZnO structure. At low Ni content $x \leq 0.05$, no additional diffraction lines resulting from Ni or NiO can be discerned. However, some weak reflections (111 and 200) of a NiO-like crystalline structure start to appear in the sample with x=0.1 and grow in intensity with increasing Ni content. After a careful inspection on the XRD patterns, we find that the Bragg angle positions depend sensitively on the Ni concentration x as shown in Fig. 1(b). Figure 1(c) compiles the XRD patterns of H_2-annealed $Zn_{1-x}Ni_xO:H$ (x =0.0 to 0.2) samples. The data show clearly that the wurtzite ZnO structure is preserved after H_2-annealing. At a Ni concentration between x=0.1 and 0.2, the NiO-related diffraction peaks disappear completely. Instead, (111) and (200) reflections from metallic Ni show up at 2θ=44.0° and 51.3°, respectively, suggesting that the NiO-like crystals were effectively reduced into Ni clusters during the H_2-annealing step.

Figure 1(d) displays the Ni-doping concentration dependence of the lattice parameters (a and c) of wurtzite ZnO structure for as-synthesized $Zn_{1-x}Ni_xO$ and H_2-annealed $Zn_{1-x}Ni_xO:H$ (x=0 to 0.2) samples denoted by solid and open data points, respectively. The dashed lines in Fig. 1(d) mark the value of the a-axis and c-axis lattice constants, i.e. a=3.2495 Å and c=5.2069 Å, respectively, in bulk ZnO.[30] For the doping region $x \leq 0.05$, we find that the lattice parameters of the as-synthesized samples to decrease almost linearly with increasing Ni content x. The magnitude of the c-parameter decrease by ~0.2% and 0.5% for x=0.05 and 0.20, respectively. Our experimental results compare favorably with a result obtained by a recent theoretical calculation, which shows that if a Zn atom is substituted by a Ni atom in the ZnO wurtzite supercell, the lattice parameters should decrease slightly by some thousands of an angstrom.[8] Our observation of an approximate linear decrease in the cell parameters with increasing Ni concentration x for $x \leq 0.05$ could also be understood based on Vegard's law, which pre-

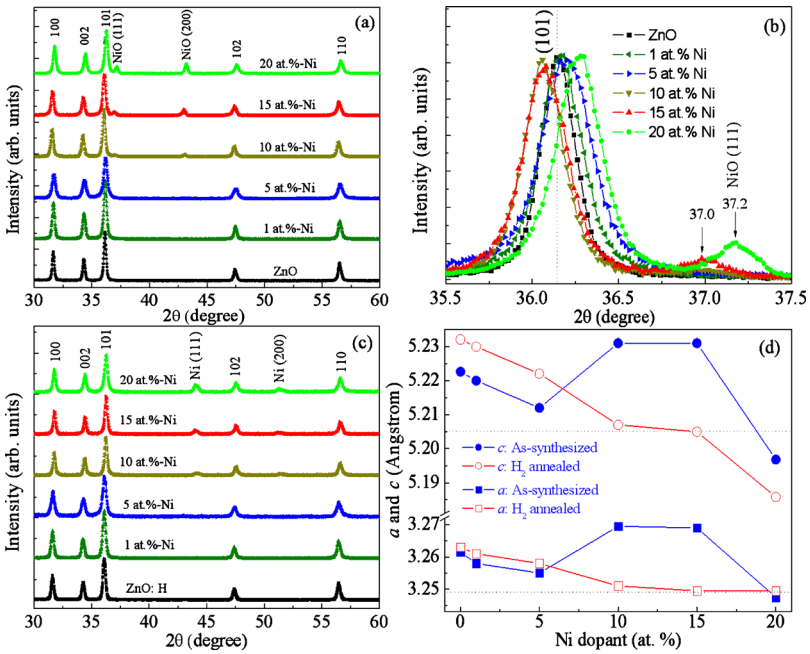

FIG. 1. (Color online) XRD patterns of [(a) and (b)] as-synthesized $Zn_{1-x}Ni_xO$ (x=0.0 to 0.2) and (c) post H_2-annealed $Zn_{1-x}Ni_xO:H$ (x=0.0 to 0.2) samples. (d) The Ni content x dependence of a-axis and c-axis lattice constants for as-prepared (solid points) and H_2-annealed (open points) samples, respectively. The dashed lines show the value of the a-axis and c-axis lattice constants, respectively, in bulk ZnO. The solid line connecting the points is a visual guide.

dicts a linear relation between the crystal lattice parameters of an alloy, such as $Zn_{1-x}Ni_xO$, and the concentrations of the constituent elements.[31]

When x increases up to 0.1, a secondary phase of tiny NiO-like crystalites is formed inside the ZnO lattice, leading to an expansion of the ZnO lattice spacing as shown in Fig. 1(d). The wurtzite ZnO has many native defects due to the lattice structure that contains large voids. Such a void can easily accommodate several Ni atoms to form a NiO-like crystallite as the Ni content x increases beyond the solid solubility limit of Ni in ZnO. When the Ni content x increases further up to x=0.2, the (111) XRD line of the NiO-like crystallites exhibits an observable right shift from 2θ =37.0° to 37.2° as shown in Fig. 1(b). The reflection peak at 2θ=37.2° corresponds closely to the line from the (111) crystal planes of bulk NiO. This indicates that a secondary phase has formed, which is related to NiO precipitated within the ZnO lattice at x=0.2, leading to a large decrease in the lattice parameters of ZnO as shown in Fig. 1(d).

With increasing Ni content x, the lattice parameters of H_2-annealed $Zn_{1-x}Ni_xO:H$ (x=0.1 and 0.2) samples exhibit a monotonously decreasing tendency, indicating that there are more Ni-ions which are incorporated in the lattice. We note that the lattice spacing of H_2-annealed samples with $x \leq 0.05$ is found to be expanded upon H_2-annealing, suggesting that hydrogen atoms have diffused into the wurtzite ZnO. Our experimental result is consistent with the previously mentioned theoretical predication based on a first-principles calculation,[32] which shows that hydrogen as a shallow donor in ZnO gives rise to large lattice relaxations. In contrast, the lattice parameters for Ni-overdoped samples with x=0.1 to 0.15 decrease significantly upon H_2-annealing. This can be understood as a consequence of a structural relaxation, which takes place when the NiO-like grains are reduced into Ni metal clusters precipitating in the ZnO lattice.

The average grain size determined from XRD (D_{101}) is estimated from the intense ZnO (101) reflection, using Scherrer's relation. The results indicate nanoparticles varying from D_{101}=31 to 48 nm for the as-synthesized material. Upon H_2-annealing, the average x-ray grain sizes decrease and vary from D_{101}=22 to 30 nm. This decrease in grain size may be mainly attributed to the desorption of excessive oxygen atoms from the surface of the as-synthesized powders during H_2-annealing as evidenced by the PL spectra measurements discussed below.

The valence states of the Ni clusters in the ZnO matrix are analyzed by means of Ni $2p$ core-level XPS spectra. Figure 2(a) shows the Ni $2p$ XPS spectrum of single-phase $Zn_{0.95}Ni_{0.05}O$ nanoparticles. The binding energies are corrected for the charging effect with reference to the C $1s$ line at 284.6 eV. The binding energies of the Ni $2p_{3/2}$ and Ni $2p_{1/2}$ photoemission lines are determined as ~855.2 eV and 872.2 eV, respectively, showing that the valence state of the Ni ions in the sample is +2.[18,33] Meanwhile, the Ni $2p_{3/2}$ main spectral feature has a satellite peak at ~861.0 eV, which is typical for the Ni^{2+} cation at tetrahedral sites within the wurtzite ZnO structure.[15,18] Figure 2(b) shows a Ni $2p$ XPS spectrum for an H_2-annealed $Zn_{0.95}Ni_{0.05}O:H$ sample.

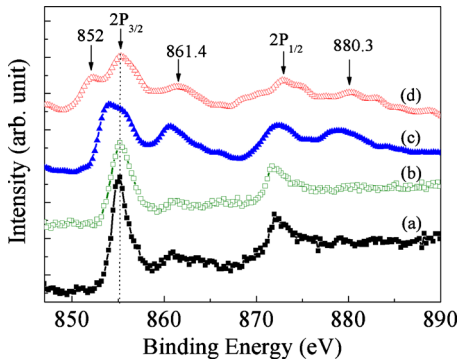

FIG. 2. (Color online) XPS patterns of (a) $Zn_{0.95}Ni_{0.05}O$, (b) $Zn_{0.95}Ni_{0.05}O:H$, (c) $Zn_{0.8}Ni_{0.2}O$, and (d) $Zn_{0.8}Ni_{0.2}O:H$ nanocrystals measured at RT.

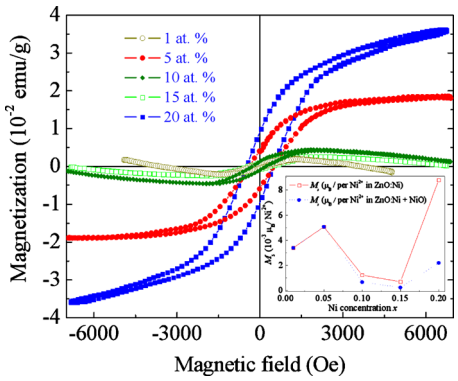

FIG. 3. (Color online) (a) Magnetic hysteresis loops of the as-synthesized $Zn_{1-x}Ni_xO$ ($x=0.01$ to 0.2) samples measured at RT. The inset shows the Ni concentration dependence of saturation magnetization M_s. The solid points denote the M_s per Ni^{2+} ion in the total samples including single-phase of ZnO:Ni and NiO, while the open points indicate the M_s per Ni^{2+} ion only in single-phase ZnO:Ni, assuming that the maximum of the solid solubility of Ni in ZnO is 5 at. % Ni. The line connecting the points is a visual guide.

The Ni $2p$ signals are similar to that of $Zn_{0.95}Ni_{0.05}O$ but the full width at half maximum value of those peaks is larger than that of $Zn_{0.95}Ni_{0.05}O$ due to inclusion of hydrogen into the ZnO lattice.

Figure 2(c) shows the Ni $2p$ XPS spectrum for the $Zn_{0.8}Ni_{0.2}O$ nanoparticles. We observe that the Ni $2p_{3/2}$ peak in $Zn_{0.8}Ni_{0.2}O$ is shifted from 855.2 to 854.0 eV due to the increase in a spectral contribution resulting from a NiO secondary phase. After H_2-annealing, a peak at 852.0 eV corresponding to metallic Ni clusters appears in the Ni $2p$ XPS spectrum for the $Zn_{0.8}Ni_{0.2}O:H$ nanoparticles as shown in Fig. 2(d). It turns out that the Ni $2p_{3/2}$ peak at 855.2 eV—corresponding to the signal from tetrahedrally bonded Ni^{2+} cations in the pure wurtzite ZnO structure—remains unchanged, while the Ni $2p_{1/2}$ signal as well as its satellite peaks related to $Zn_{0.8}Ni_{0.2}O:H$ are shifted to a higher energy position by 0.8 eV after H_2-annealing. The increase in the energy separation between Ni $2p_{3/2}$ and $2p_{1/2}$ peaks may be related to an increase in the tetrahedral crystal field of ZnO when the unit cell parameters decrease upon H_2-annealing.

B. Magnetic properties

Figure 3 compares the magnetic hysteresis (M-H) loops measured at RT for the as-synthesized $Zn_{1-x}Ni_xO$ ($x=0.01$ to 0.20) powders. All the curves are characteristic of ferromagnetic behavior with the coercive field about 400 Oe. The magnitude of the saturation magnetization observed here is comparable with previous reports in Ni-doped ZnO powders prepared by chemical methods.[12,16] The inset in Fig. 3 shows the Ni concentration dependence of the saturation magnetization (M_s) of the samples. The solid data points denote the average M_s values per Ni^{2+} ion in the samples including the primary ZnO:Ni phase and the secondary NiO phase, while the open data points indicate the saturation magnetization M_s per Ni^{2+} ion for the single-phase wurtzite ZnO:Ni only, assuming that the maximum of the solid solubility of Ni in ZnO is 5 at. % Ni. The line connecting the points is a guide to the eye. We see that the M_s values first increase at low Ni content $x \leq 0.05$, and then decrease at medium Ni content stage ($x=0.1$ to 0.15), before they increase again at $x=0.2$. The increase in M_s with the nickel content at $x \leq 0.05$ can be attributed to a progressive increase in the ferromagnetic interactions, being related to a decrease in the average distance between the Ni^{2+} ions as x increases. With further increase in the Ni concentration up to $x=0.10$ and 0.15, the magnetic moment decreases. Such a decrease was also observed[15] previously in Ni-doped ZnO films at high doping level. It was attributed to a preference of antiferromagnetic over ferromagnetic interactions of Ni ions as the average distance between adjacent Ni^{2+} ions in the single-phase of the wurtzite ZnO:Ni lattice decreases. However, this mechanism cannot explain our results on the overdoped samples. In our system, the expanded wurtzite ZnO:Ni lattice due to the precipitation of NiO-like crystallites could be a main reason for the decrease in M_s at $x=0.1$ and 0.15. Recent electronic structure calculations suggest that strong atomic hybridization between Ni $3d$ states and O $2p$ states produces a long-range ferromagnetic coupling among all Ni dopant atoms in the ZnO:Ni semiconductor.[8] The enlarged wurtzite ZnO:Ni lattice may modify the sp-d hybridization and may change the energy difference between ferromagnetic and antiferromagnetic coupling states of adjacent Ni^{2+} ions and may thus lead to a change in magnetic ordering. This assumption is also supported by recent theoretical calculation by Gopal and Spaldin.[34] The authors showed that the magnetic configuration in TM-doped ZnO is sensitive to the amount of lattice relaxation. At $x=0.2$, the segregation of NiO crystals from the wurtzite ZnO:Ni lattice results in a significant contraction of the ZnO:Ni lattice and thus a large increase in the FM in ZnO:Ni nanoparticles. As we can see in Fig. 3, the as-synthesized $Zn_{0.8}Ni_{0.2}O$ sample shows a clear enhanced ferromagnetic behaviour at low fields and a superparamagnetic-like behaviour at high fields. This magnetic two-phase behavior may also be related to the different crystalline phases. The ferromagnetic behaviour can be attributed to the intrinsic properties of single-phase ZnO:Ni nanocrystallites, while the superparamagnetic behaviour may be attributed to NiO-like nanoparticles, which is also consistent with previous reports.[16,35]

Figure 4 shows some typical magnetic hysteresis loops obtained from as-synthesized $Zn_{1-x}Ni_xO$ and post H_2-annealed $Zn_{1-x}Ni_xO:H$ nanocrystal composites with $x=0.05$ and 0.20, respectively. As displayed in Fig. 4(a), the H_2-annealed $Zn_{0.95}Ni_{0.05}O:H$ sample reveals an enhanced saturation magnetization with increased coercivity $H_c=500$ Oe. The increase in the coercivity value from $H_c=400$ to 500 Oe may be related to H impurities or defects created during H_2-annealing. These inhomogeneities may serve as pinning sites to impede the domain wall motion and thus enhance the coercivity of the magnetic powders. We also note that the hysteresis loop of the $Zn_{0.95}Ni_{0.05}O:H$ sample also exhibits a superparamagnetic-like behaviour at high fields. This is due to a finite-size effect as evidenced from XRD measurements showing that the H_2-annealing induces decrease in average x-ray grain size from $D_{101}=31$ nm down to 22 nm. It is worth mentioning that the H_2-annealing induced enhancement of the saturation magnetization observed at high fields is not as large as that reported

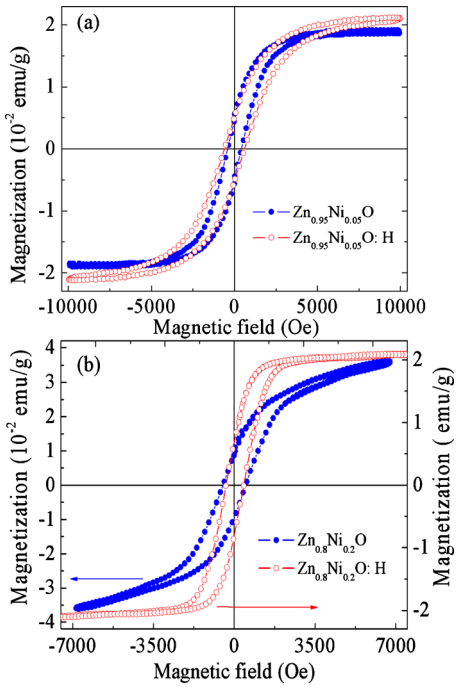

FIG. 4. (Color online) Magnetic hysteresis loops of as-synthesized (solid point) and post H_2-annealed (open point) $Zn_{1-x}Ni_xO$:H samples with (a) $x=0.05$, (b) $x=0.2$, respectively.

in the Co-doped ZnO films[26] or V-doped ZnO powders.[29] This may be understood by the combined effects of H_2-annealing induced increase in free carrier concentration and the large lattice relaxation. As mentioned above, the enlarged cell lattice spacing due to the incorporation of interstitial H into the ZnO:Ni lattice may weaken the *sp-d* hybridization and reduce the ferromagnetic coupling between neighboring magnetic Ni^{2+} irons. This effect may partially offset the H-mediated enhancement of FM due to the increase in hydrogen concentration.

Figure 4(b) compiles the magnetic hysteresis (*M-H*) loops of $Zn_{0.8}Ni_{0.2}O$ and $Zn_{0.8}Ni_{0.2}O$:H samples measured at RT. As expected, the H_2-annealed $Zn_{0.8}Ni_{0.2}O$:H sample shows a strongly enhanced FM with a saturation magnetization value of ~2.1 emu/g, which is about two orders of magnitude larger than that of the as-prepared sample. Combining our XRD and XPS results, we conclude that such a large enhancement of RT-FM could be related mainly to the precipitating metal Ni clusters.

C. Optical properties

PL spectroscopy is a powerful tool to characterize the structural defects, which have been shown to play a crucial role in the development of ferromagnetic properties in ZnO-based DMSs. In order to further understand the occurrence of FM in Ni-doped ZnO, we restrict our study to the single-phase compounds of $Zn_{1-x}Ni_xO$ with $x \leq 0.05$. In Fig. 5, we show our RT PL spectra taken from the as-synthesized single-phase wurtzite $Zn_{1-x}Ni_xO$ ($x \leq 0.05$) samples. The PL spectra display an evident excitonic UV emission and a broad feature with multiple subpeaks in the visible emission region spanning the range from green to red. The UV emission is well understood as a near-band edge (NBE) exciton

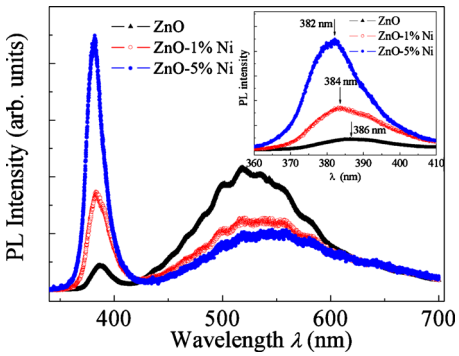

FIG. 5. (Color online) RT PL spectra of the as-prepared $Zn_{1-x}Ni_xO$ ($x=0$, 0.01, and 0.05) samples. The inset shows the blueshift in the NBE emission.

emission arising from the recombination of photogenerated charge carriers across the band gap of ZnO, while a variety of deep-level defects have been proposed as possible contributors to the emission in the visible regime. Recent reports have attributed the green light emission centered at 494 nm (2.51 eV) to an oxygen vacancy (V_O),[36] the emission feature at 520 nm (2.38 eV) to antisite oxide (O_{Zn}),[37] whereas the yellow to red emission contributions from 540 to 700 nm are attributed to oxygen interstitials (O_i).[38] It is generally believed that the UV emission intensity at RT is related to a variation in electron concentration,[39] while the visible emission intensity correlates directly with intrinsic defect densities in the material. It is shown in Fig. 5 that with increasing Ni concentration the UV emission intensity increases, while the visible emission for wavelengths between 450 and 600 nm decreases. We conclude that the Ni-doping leads to an increase in the electron concentration and a concomitant decrease in the intrinsic defects (such as V_O and O_{Zn}) density.

It should be noted that the NBE emission peak blueshifts as the Ni concentration increases for the $Zn_{1-x}Ni_xO$ powders with low Ni concentration of $x \leq 0.05$ as shown in the inset of Fig. 5. This blueshift behavior can in principle be explained by the Moss–Burstein band filling effect.[40,41] The Burstein–Moss effect is frequently observed in n-type semiconductors.[42,43] Electron-doped ZnO with a high concentration of n-type carriers is easily achievable, because intrinsic defects in ZnO may render it naturally n-type.[23,44] An increase in the carrier concentration in Ni-doped ZnO will cause the Fermi level to move into the conduction band. The filling of the conduction band by electrons will generally result in a blueshift in the NBE emission.[45] The magnitude of the shift (ΔE^{BM}), under free-electron theory, is described as

$$\Delta E^{BM} = \frac{h^2}{8\pi^2 m^*}(3\pi^2 n_e)^{2/3}, \quad (1)$$

where h is Plank's constant, m^* is the reduced effective mass derived from the valence and conduction band effective masses, m_v^* and m_c^*, according to $(1/m^*)=(1/m_v^*)+(1/m_c^*)$, and n_e is the electron carrier concentration.

Figure 6(a) displays the DR spectra of single-phase $Zn_{1-x}Ni_xO$ ($x \leq 0.05$) nanoparticles. As can be seen in this figure, the undoped ZnO powder shows high DR values of about 80% over the wavelength range from 400 to 800 nm. A strong absorption band is observed at wavelengths smaller

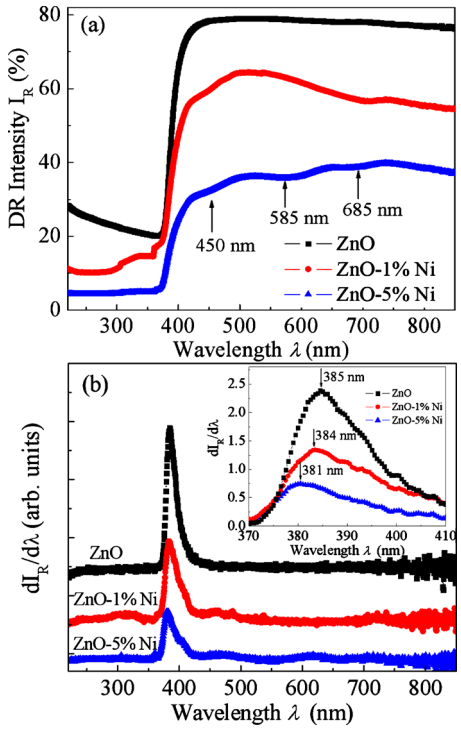

FIG. 6. (Color online) (a) RT DR spectra and (b) the $dI_R/d\lambda$ vs wavelength plots of as-prepared $Zn_{1-x}Ni_xO$ (x=0, 0.01, and 0.05) samples. The inset shows the blueshift in the absorption edge.

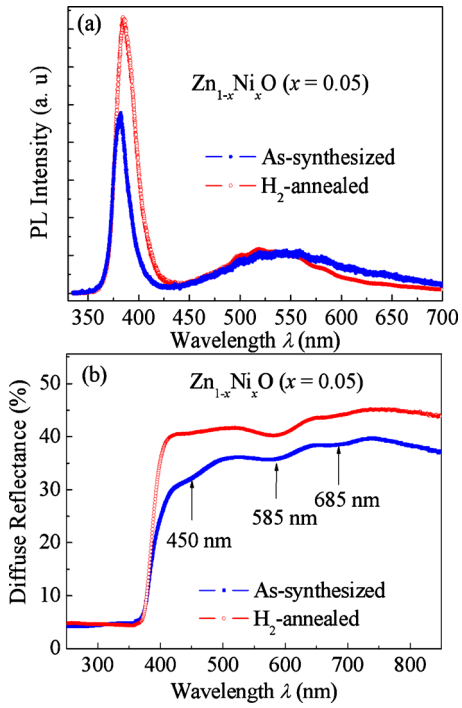

FIG. 7. (Color online) (a) PL spectra and (b) DR spectra of as-synthesized (solid data) and H_2-annealed (open data) $Zn_{0.95}Ni_{0.05}O:H$ samples.

than 400 nm, which corresponds to the direct band gap of ZnO. Figure 6(b) shows the $dI_R/d\lambda$ versus λ plots for revealing the absorption edge clearly. The inset shows the positions of the maximum absorption change in electronic transition as denoted by arrows. It is found that the blueshifts in the absorption edge are comparable with the Moss–Burstein shifts in the NBE emission. A long-tail background DR in the spectra for wavelengths below the band gap is mainly due to the presence of oxygen-related defects such as O_V and O_{Zn} or O_i as evidenced from the PL data. The variation in the DR spectra for the Ni-doped samples as compared with the undoped sample is an indication of the incorporation of Ni ions in the ZnO lattice. In the DR spectra of Ni-doped samples, additional absorption bands are observed around 450, 585, and 685 nm, which are consistent with earlier reports.[14,22,46] These absorption bands could be assigned as typical $d-d$ transitions of high-spin states of Ni^{2+} ions (configuration being $3d^8$) in a tetrahedral oxygen coordination. The magnetic impurity d-states of Ni^{2+} ions split under the influence of the tetrahedral crystal field of ZnO, leading to a lower doublet e_g state and a higher energy triplet t_{2g} state. The electronic ground state, ^3F, splits into three states $^3A_2(F)$, $^3T_2(F)$, and $^3T_1(F)$, whereas the excited state "^3P" becomes $^3T_1(P)$, such that its energy level lies below $^3A_2(F)$. The possible $d-d$ transitions can, therefore, take place from $^3T_1(F)$ to $^3A_2(F)$, $^3T_1(P)$, and $^3T_2(F)$. A series of observed optical absorption bands can be attributed to these $d-d$ transitions arising due to presence of midband gap states.[14,22,46] The observation of these characteristic absorption bands indicates again that Ni^{2+} ions are substituting Zn^{2+} ions in the tetrahedral ZnO environment.

Annealing at 400 °C for 2 h in hydrogen atmosphere of 1 atm caused a large increase in the UV emission intensity and a concomitant quenching of the visible emission (particularly the yellow and red emission) as shown in Fig. 7(a). Recent studies show that the origin of UV emission at RT is related to the electron concentration in ZnO,[39] and it was demonstrated that hydrogenation can increase the carrier concentration significantly, thus enhancing donor-bound exciton PL emission.[47] Therefore, the large enhancement of the UV emission observed here may be attributed to the increase in the hydrogen impurity concentration in ZnO upon H_2-annealing. The quenching of the yellow and red emission indicates a decrease in the O_i density probably due to desorption of excessive oxygen from the nanoparticles and especially from the surface of the powders.

Figure 7(b) shows the DR spectra of the $Zn_{0.95}Ni_{0.05}O$ and $Zn_{0.95}Ni_{0.05}O:H$ samples in the range of 250–850 nm. We observe that after H_2-annealing the DR intensity in the long wavelengths range above 400 nm increases significantly and the absorption edge around 400 nm becomes steeper. This could be caused by an improved stoichiometry of the chemical composition of ZnO due to decrease in oxygen interstitials defects in $Zn_{0.95}Ni_{0.05}O:H$ sample as evidenced from above PL measurements.

In summary, we have shown that with increasing Ni dopant concentration the UV emission intensity of single-phase ZnO:Ni increases and is accompanied by a UV peak blueshift, while the dominant green emission intensity decreases with increasing Ni dopant. The blueshift and the enhancement of the UV emission intensity upon Ni and Ni–H doping are attributed to the increase in the free carrier concentration in the conduction band of ZnO:Ni, which is consistent with the Ni-doping induced enhancement of FM. The obvious cor-

relation between the FM and carrier concentration in Ni and Ni–H doped ZnO suggests that this effect contributes to the mechanism of carrier-mediated FM for Ni-doped ZnO DMSs.

IV. CONCLUSIONS

The effects of H_2-annealing on the crystal structure and magnetic properties of Ni-doped ZnO powders have been investigated systematically. The main conclusions are summarized as following.

(1). The XRD data analysis reveals that the Ni-doping process contains three stages, namely, (a) single-phase stage of wurtzite ZnO at low Ni content $x \leq 0.05$, (b) an initial stage of a secondary phase of NiO-like crystallites formed inside the ZnO lattice at medium Ni content $x = 0.1$ and 0.15, and (c) a phase-separation stage of NiO crystallites precipitated in the ZnO host lattice at $x = 0.2$.

(2). We demonstrate correlations between structural parameters and FM at three doping stages. At the single-phase and phase segregation stages, proper Ni-doping into the ZnO lattice leads to a decrease in the lattice parameters and consequently an enhancement of the FM. At intermediate Ni content $x = 0.1$ and 0.15, NiO-like crystallites form and distort the ZnO host lattice towards larger lattice spacing, resulting in a deterioration of the FM in ZnO:Ni DMSs.

(3). XRD, XPS, VSM, PL, and DR spectrum measurements indicate that Ni^{2+} ions are substituting Zn^{2+} ions at the Zn sites in the ZnO lattice at low Ni concentrations of $x \leq 0.05$. The exchange interactions between Ni^{2+} ions mediated by free carriers contribute to the FM at RT.

(4). Upon H_2-annealing the single-phase $Zn_{1-x}Ni_xO:H$ samples with $x \leq 0.05$ show an increase in both coercivity and saturation magnetization. The PL and DR spectrum data suggest that the hydrogen shallow donors and an improved sample quality may be responsible for the H_2-annealing induced enhancement of RT-FM.

(5). Upon H_2-annealing, a huge enhancement of M_s observed in highly doped samples ($x = 0.1$ to 0.2) is mainly related to the formation of Ni clusters reduced from NiO crystallies.

Our consistent and robust experimental data presented here are crucial for both an improvement and testing of the theoretical models and for further experimental approaches aiming at the opportunity to develop spintronic devices based on Ni-doped ZnO.

ACKNOWLEDGMENTS

This work has been supported by the scientific research foundation for the returned overseas Chinese scholars, State Education Ministry, and the Natural Science Foundation of Anhui Province, China (Grant No. 070414197) and NSFAP for Excellent Youth through Grant No. 08040106823.

[1]J. M. D. Coey, M. Venkatesan, and C. B. Fitzgerald, Nature Mater. **4**, 173 (2005).
[2]S. A. Wolf, D. D. Awschalon, R. A. Buhrman, J. M. Daughton, S. Von Molnar, M. L. Roukes, A. Y. Chtchelkanova, and D. M. Treger, Science **294**, 1488 (2001).
[3]T. Dietl, H. Ohno, and F. Matsukura, Science **287**, 1019 (2000).
[4]S. Kolesnik, B. Dabrowski, and J. Mais, J. Appl. Phys. **95**, 2582 (2004).
[5]D.-L. Hou, X.-J. Ye, H.-J. Meng, H.-J. Zhou, X.-L. Li, C.-M. Zhen, and G.-D. Tang, Appl. Phys. Lett. **90**, 142502 (2007).
[6]Y. Matsumoto, M. Murakami, T. Shono, T. Hasegawa, T. Fukumura, M. Kawasaki, P. Ahmet, T. Chikyow, K. Shin-ya, and H. Koinuma, Science **291**, 854 (2001).
[7]K. Sato and H. Katayama-Yoshida, Jpn. J. Appl. Phys., Part 2 **39**, L555 (2000); Physica E (Amsterdam) **10**, 251 (2001).
[8]R. G. Hernández, W. L. Pérez, and M. J. A. Rodríguez, J. Magn. Magn. Mater. **321**, 2547 (2009).
[9]M. Venkatesan, C. B. Fizgerald, J. G. Lunney, and J. M. D. Coey, Phys. Rev. Lett. **93**, 177206 (2004).
[10]X. X. Liu, F. T. Lin, L. L. Sun, W. J. Cheng, X. M. Ma, and W. Z. Shi, Appl. Phys. Lett. **88**, 062508 (2006).
[11]P. V. Radovanovic and D. R. Gamelin, Phys. Rev. Lett. **91**, 157202 (2003).
[12]C. J. Cong, J. H. Hong, Q. Y. Liu, L. Liao, and K. L. Zhang, Solid State Commun. **138**, 511 (2006).
[13]W. Yu, L. H. Yang, X. Y. Teng, J. C. Zhang, Z. C. Zhang, L. Zhang, and G. S. Fu, J. Appl. Phys. **103**, 093901 (2008).
[14]S. Thota, L. M. Kukreja, and J. Kumar, Thin Solid Films **517**, 750 (2008).
[15]D.-L. Hou, R.-B. Zhao, Y.-Y. Wei, C.-M. Zhen, C.-F. Pan, and G.-D. Tang, Curr. Appl. Phys. **10**, 124 (2010).
[16]M. El-Hilo, A. A. Dakhel, and A. Y. Ali-Mohamed, J. Magn. Magn. Mater. **321**, 2279 (2009).
[17]T. Wakano, N. Fujimura, Y. Morinaga, N. Abe, A. Ashida, and T. Ito, Physica E (Amsterdam) **10**, 260 (2001).
[18]Z. Yin, N. Chen, F. Yang, S. Song, C. Chai, J. Zhong, H. Qian, and K. Ibrahim, Solid State Commun. **135**, 430 (2005).
[19]S. K. Mandal, A. K. Das, T. K. Nath, and D. Karmakar, Appl. Phys. Lett. **89**, 144105 (2006).
[20]X. J. Liu, X. Y. Zhu, C. Song, F. Zeng, and F. Pan, J. Phys. D: Appl. Phys. **42**, 035004 (2009).
[21]X. Mao, W. Zhong, and Y. Du, J. Magn. Magn. Mater. **320**, 1102 (2008).
[22]M. Snure, D. Kumar, and A. Tiwari, Appl. Phys. Lett. **94**, 012510 (2009).
[23]C. H. Park and D. J. Chadi, Phys. Rev. Lett. **94**, 127204 (2005).
[24]H. J. Lee, C. H. Park, S. Y. Jeong, K. J. Yee, C. R. Cho, M. H. Jung, and D. J. Chadi, Appl. Phys. Lett. **88**, 062504 (2006).
[25]S. Deka and P. A. Joy, Appl. Phys. Lett. **89**, 032508 (2006).
[26]H. S. Hsu, J. C. A. Huang, S. F. Chen, and C. P. Liu, Appl. Phys. Lett. **90**, 102506 (2007).
[27]Z. H. Wang, D. Y. Geng, S. Guo, W. J. Hu, and Z. D. Zhang, Appl. Phys. Lett. **92**, 242505 (2008).
[28]B. K. Roberts, A. B. Pakhomov, and K. M. Krishnan, J. Appl. Phys. **103**, 07D133 (2008).
[29]S. H. Liu, H. S. Hsu, C. R. Lin, C. S. Lue, and J. C. A. Huang, Appl. Phys. Lett. **90**, 222505 (2007).
[30]C. Liu, S. H. Chang, T. W. Noh, M. Abouzaid, P. Ruterana, H. H. Lee, D.-W. Kim, and J.-S. Chung, Appl. Phys. Lett. **90**, 011906 (2007).
[31]L. Vegard, Z. Phys. **5**, 17 (1921).
[32]C. G. Van de Walle, Phys. Rev. Lett. **85**, 1012 (2000).
[33]H. Wang, Y. Chen, H. B. Wang, C. Zhang, F. J. Yang, J. X. Duan, C. P. Yang, Y. M. Xu, M. J. Zhou, and Q. Li, Appl. Phys. Lett. **90**, 052505 (2007).
[34]P. Gopal and N. A. Spaldin, Phys. Rev. B **74**, 094418 (2006).
[35]J. T. Richardson, D. I. Yiagas, B. Turk, K. Forster, and M. V. Twigg, J. Appl. Phys. **70**, 6977 (1991).
[36]Z. Yan, Y. Ma, D. Wang, J. Wang, Z. Gao, L. Wang, P. Yu, and T. Song, Appl. Phys. Lett. **92**, 081911 (2008).
[37]B. X. Lin, Z. X. Fu, and Y. B. Jia, Appl. Phys. Lett. **79**, 943 (2001).
[38]Y. Sun, N. G. Ndifor-Angwafor, D. Jason Riley, and M. N. R. Ashfold, Chem. Phys. Lett. **431**, 352 (2006).
[39]H. S. Kang, G. H. Kim, S. H. Lim, H. W. Chang, J. H. Kim, and S. Y. Lee, Thin Solid Films **516**, 3147 (2008).
[40]E. Burstein, Phys. Rev. **93**, 632 (1954).
[41]T. S. Moss, Proc. Phys. Soc. London, Sect. B **67**, 775 (1954).
[42]S. Suwanboon, P. Amornpitoksuk, A. Haidoux, and J. C. Tedenac, J. Alloys Compd. **462**, 335 (2008).
[43]T. Rattana, S. Suwanboon, P. Amornpitoksuk, A. Haidoux, and P. Limsuwan, J. Alloys Compd. **480**, 603 (2009).
[44]D. C. Look, J. W. Hemsky, and J. R. Sizelove, Phys. Rev. Lett. **82**, 2552

(1999).
[45]F. K. Shan, G. X. Liu, W. J. Lee, and B. C. Shin, J. Cryst. Growth **291**, 328 (2006).
[46]S. Singh, N. Rama, and M. S. Ramachandra Rao, Appl. Phys. Lett. **88**, 222111 (2006).
[47]Y. M. Strzhemechny, H. L. Mosbacker, D. C. Look, D. C. Reynolds, C. W. Litton, N. Y. Garces, N. C. Giles, L. E. Halliburton, S. Niki, and L. J. Brillson, Appl. Phys. Lett. **84**, 2545 (2004).